



OPEN

Numerical assessment of irreversibility in radiated Sutterby nanofluid flow with activation energy and Darcy Forchheimer

Mujeeb ur Rahman¹, Fazal Haq¹✉, M. Ijaz Khan^{2,3,4}, Fuad A. Awwad⁵ & Emad A. A. Ismail⁵

Entropy generation is a concept that is primarily associated with thermodynamics and engineering, and it plays a crucial role in understanding and optimizing various processes and systems. Applications of entropy generation can be seen in turbo machinery, reactors, chillers, desert coolers, vehicle engines, air conditioners, heat transfer devices and combustion. Due to industrial applications entropy generation has gained attention of researchers. Owing such applications, current communication aims to model and analyzed the irreversibility in Sutterby nanofluid flow by stretched cylinder. Momentum equation is reported by considering porosity, Darcy Forchheimer and magnetic field. While in energy equation radiation and Joule heating effects are accounted. Activation energy impact is accounted in the modeling of concentration equation. Thermodynamics second law is utilized for physical description of irreversibility analysis. Through similarity transformations dimensional equations representing flow are transformed to dimensionless ones. Numerical solution for ordinary system is obtained via Runge–Kutta–Fehlberg scheme in Mathematica platform through NDSolve code. Influence of prominent variables on velocity, entropy, temperature, Bejan number and concentration are graphically analyzed. Coefficient of skin friction, gradient of temperature and Sherwood number are numerically analyzed. The obtained results show that velocity field decreases through higher porosity and Forchheimer variables. Velocity and temperature curves shows an opposite trend versus magnetic parameter. A decay in concentration distribution is noticed through larger Schmidt number. Entropy generation amplifies against magnetic parameter and Brinkman number.

List of symbols

m	Power law index (–)
k	Thermal conductivity ($\text{W m}^{-1}\text{K}^{-1}$)
τ	Heat capacity ratio (–)
B_0	Strength of magnetic field ($\text{kg s}^{-2}\text{A}^{-1}$)
μ	Fluid friction ($\text{kg m}^{-1}\text{s}^{-1}$)
D_T	Thermophoresis dispersion ($\text{m}^2 \text{s}^{-1}$)
ρ	Density of fluid (kg m^{-3})
(u, w)	Velocity components (ms^{-1})
T	Temperature (K)
σ^*	Stefan Boltzmann constant ($\text{J s}^{-1}\text{m}^{-2} \text{K}^{-4}$)
C_∞	Ambient concentration (–)
k_r^2	Chemical reaction rate (s^{-1})

¹Department of Mathematical Sciences, Karakoram International University, Gilgit 15100, Pakistan. ²Department of Mathematics, Riphah International University, Islamabad Campus, Islamabad 44000, Pakistan. ³Department of Mechanical Engineering, Lebanese American University, Kraytem, Beirut 1102-2801, Lebanon. ⁴Department of Mechanics and Engineering Science, Peking University, Beijing 100871, China. ⁵Department of Quantitative Analysis, College of Business Administration, King Saud University, P.O. Box 71115, 11587 Riyadh, Saudi Arabia. ✉email: fazal.haq@kiu.edu.pk

D_B	Brownian motion coefficient ($\text{m}^2 \text{s}^{-1}$)
τ_w	Shear stress (Wm^{-2})
J_w	Mass flux (ms^{-1})
$\theta(\eta)$	Temperature (—)
R	Radius of cylinder (m)
Pr	Prandtl variable (—)
λ	Porosity parameter (—)
Re	Reynolds number (—)
Rd	Radiation parameter (—)
Nt	Thermophoretic diffusion variable (—)
δ_1	Temperature difference ratio parameter (—)
γ	Rate of chemical reaction (—)
ν	Kinematic viscosity ($\text{m}^2 \text{s}^{-1}$)
B	Characteristic time (s)
σ	Electric conductivity ($\text{kg}^{-1} \text{m}^{-3} \text{s}^3 \text{A}^2$)
k_p	Porous medium permeability (m^2)
F_e	Inertial coefficient (kgm^2)
k^*	Coefficient of mean absorption (m^{-1})
D_B	Brownian movement ($\text{m}^2 \text{s}^{-1}$)
E_a	Activation energy ($\text{kg m}^2 \text{s}^{-2}$)
C_p	Specific heat ($\text{J kg}^{-1} \text{K}^{-1}$)
n_1	Fitted rate constant (—)
(r, z)	Coordinate axes (m)
T_∞	Ambient temperature (K)
C	Concentration (—)
q_w	Heat flux (J s^{-2})
$f'(\eta)$	Velocity
$\phi(\eta)$	Concentration (—)
γ_3	Curvature variable (—)
M	Magnetic variable (—)
β_1	Sutterby fluid parameter (—)
Fr	Forchheimer variable (—)
Nb	Brownian dispersion variable (—)
E_1	Activation energy parameter (—)
Ec	Eckert number (—)
Sc	Schmidt number (—)

Viscoelastic liquids like molten polymers and polymer solutions exhibit numerous verities of rheological characteristics. These features include time dependent viscosity, shear rate dependent viscosity, normal stresses in steady shear flow and various time-dependent elastic effects. Sutterby fluid model is one of the most important models proposed by Sutterby¹, which addresses the solution of high polymer aqueous solutions. Imran et al.² inspected the thermal radiation and chemical reaction influences on Sutterby nanomaterial flow in inclined elastic channel. Impact of radiation, mixed convection and Joule heating on Sutterby nanoliquid flow in a vertical channel is numerically examined by Hayat et al.³. Akbar and Nadeem⁴ reported mixed convection flow of Sutterby nanoliquid in a diverging tube. Helical flow of Sutterby nanomaterial between two concentric cylinders is scrutinized by Batra and Eissa⁵. Ishtiaq et al.⁶ examined shear thickening/thinning behavior of Sutterby nanomaterial flow over biaxially stretchable sheet with magnetic field and heat source/sink. Mixed convection and Arrhenius kinetics effects on 3-D steady flow of Sutterby nanomaterial is conveyed by Azam et al.⁷. Khan et al.⁸ inspected the features of stratified Sutterby nanomaterial flow in presence of external radiation and Lorentz force.

Mixture of nano-sized metallic particles and base fluids are nanofluids/nanomaterials. Nano-sized metallic particles include metallic oxides, metals, carbon nanotubes and nitrides. Conventional base fluids are water, ethylene glycol and light oils. Nanofluids have higher thermal performance as compared to conventional carrier liquids. Practical usages of such nanofluids can be seen in thermal engineering processes like fuel cells, refrigerators and engine oil. Firstly Choi⁹ added nano-sized metallic particles in carrier fluids and concluded that thermal features improved significantly. Buongiorno¹⁰ provided a model to study heat transfer augmentation in nanomaterials. He considered seven slip mechanisms for nanoparticles and proved that thermophoresis diffusion and Brownian movement are governing factors as compared to others. Prasad et al.¹¹ reported radiative nanofluid flow with Lorentz force effect. Turkyilmazoglu¹² inspected mass and heat transportation in nanofluid flow over different frames using Buongiorno model. Tian et al.¹³ analyzed convectively heated MHD nanoliquid flow having stagnation point over stretching sheet. Features of laminar flow of viscous fluid flow by stretchable cylinder are analytically examined by Turkyilmazoglu¹⁴. Hayat et al.¹⁵ analyzed convective hybrid nanofluid flow with radiation and heat transfer characteristics. Influences of Hall current and electrical MHD in flow of micropolar nanofluid between a pair of rotating disks is explored by Awan et al.¹⁶. Hussain et al.¹⁷ inspected features of rotating flow of hybrid nanoliquid accounting the influences of restricted slip boundary constraints. Qureshi et al.¹⁸ examined impressions of heat generation and magnetic field in hybrid peristaltic flow in a metachronal wave. Parveen et al.¹⁹ inspected the characteristics of dissipative bioconvective flow of nanoliquid which contains chemotactic microorganisms through Joule heating. Rheological properties of Pseudo plastic nanomaterial flow in a symmetric channel accounting the effects of ciliary motion is presented by Khan et al.²⁰.

Bayesian regularization networks is implemented to explore the features of nanofluid flows considering various effects by Awan et al.^{21,22}. Ahmad et al.²³ deliberated Maxwell nanomaterial flow by permeable rotating frame with heat transfer analysis. Flow behavior of radiative MHD Maxwell nanoliquid considering viscous dissipation effects is investigated by Hsiao²⁴. Hassan et al.²⁵ inspected the behavior of MHD hybrid nanomaterial flow which contains SWCNT-Ag as nanoparticles with radiation effects. A few more studies related to nanofluid are given in refs.^{26–30}

Due to applications in environmental, chemical, industrial and pharmaceutical sectors nanoliquid flows over porous surface have gained significance. Applications of such flows may include in energy storage units, geothermal heat exchanger layouts, nuclear waste disposal and crude oil production. Seddeek³¹ reported convective nanofluid flow having thermophoresis and dissipation features saturating porous space. Umavathi et al.³² described Darcy-Forchheimer convective nanofluid flow with Brinkman relation. Muhammad et al.³³ analyzed Maxwell nanoliquid flow in Darcy-Forchheimer porous space. Hayat et al.³⁴ scrutinized Darcy-Forchheimer flow with carbon nanotubes in presence of permeability. Alzahrani³⁵ investigated bidirectional flow of CNTs in Darcy-Forchheimer and porous surface. Turkyilmazoglu³⁶ studied the features magnetic field of uniform strength applied horizontally to the flow generated by rotating disk. Hayat et al.³⁷ discovered Carreau nanoliquid flow due to heated surface with Darcy-Forchheimer and porosity effects.

In chemical reactions role of activation energy (AE) is noteworthy. The lowest energy amount obligatory to trigger a chemical reaction is named as AE. In different fields AE concept is widely used such as water mechanics, oil emulsions and oil tank counting. Bestman³⁸ revealed flow over porous surface in existence of energy activation and binary response with mass and heat transmission characteristics. Makinde et al.³⁹ reported steady radiative flow over porous medium with heat transfer and chemical reaction impacts in an optically reedy atmosphere. Maleque⁴⁰ discovered unsteady boundary layer flow having heat sink/source and energy activation impacts. Awad et al.⁴¹ investigated unsteady rotational viscid fluid flow considering AE and chemical reaction. Impacts of AE and thermal radiation on MHD flow of Carreau are reported by Hsiao⁴².

Entropy generation (EG) is an extensive property of thermodynamics. Thermodynamics second law states that in an isolated thermal system entropy never decays. In an irreversible reaction total entropy always increases while in reversible reactions it remains constant. Bejan⁴³ studied irreversibility in convective nanoliquid flow. Turkyilmazoglu⁴⁴ scrutinized EG and slip impressions in radiated fluid flow in by metallic permeable channel. Khan et al.⁴⁵ calculated the EG in radiative flow of Sisko liquid by stretched surface with dissipation effect. Vatanmakan et al.⁴⁶ examined EG in steam flow with volumetric heating and turbine blades. Hayat et al.⁴⁷ inspected EG in Casson type nanoliquid flow by stretchable sheet through magnetic field and Arrhenius kinetics. Gul et al.⁴⁸ reported EG in viscoelastic Poiseuille nanofluid flow. Xie and Jian⁴⁹ discussed entropy optimization rate in MHD nanofluid flow through micro parallel networks. Khan et al.⁵⁰ scrutinized irreversibility in rotational viscous nanofluid flow with mixed convection and radiative heat flux. Huminic and Huminic⁵¹ reported irreversibility in hybrid nanomaterials flow.

The literature cited in above transpires that irreversibility in Darcy Forchheimer flow of Sutterby nanomaterial due to stretched cylinder with porous walls in existence of Arrhenius kinetics, Joule heating and chemical reaction is not examined till now. In order to fill this gape, motivation here is to investigate the irreversibility in radiative Sutterby nanoliquid flow by stretchable cylinder. Heat transport characteristics are scrutinized through Joule hating and radiation effects. Furthermore, Brownian movement and thermophoresis diffusion impacts are accounted. Mass transfer characteristics are reported through activation energy. Utilizing thermodynamics second law physical description of irreversibility is analyzed.

Problem description

In current inspection, incompressible steady flow of Sutterby nanomaterial by stretchable cylinder is considered. The flow is taken along axial z -direction and radial direction is taken normal to z -direction. The cylinder stretches with velocity $U_w = \frac{U_0 z}{l}$ in the axial direction due which flow generates. Magnetic field of constant strength B_0 is imposed vertical to the flow. Induced magnetic field effect is neglected for small Reynolds number. Effects of Arrhenius kinetics, Joule heating and radiation have been incorporated in thermal and mass concentration equations. Boundary layer conventions are accounted in development of flow governing model equations. Schematic flow diagram with boundary restrictions is depicted in Fig. 1. The governing equations signifying the flow under above norms are as follows^{52,53},

$$\frac{\partial u}{\partial r} + \frac{u}{r} + \frac{\partial w}{\partial z} = 0, \quad (1)$$

$$u \frac{\partial w}{\partial r} + w \frac{\partial w}{\partial z} = \frac{\nu}{2r} \frac{\partial w}{\partial r} + \frac{\nu}{2} \frac{\partial^2 w}{\partial r^2} - \frac{\nu m B^2}{4} \left(\frac{\partial w}{\partial r} \right)^2 \frac{\partial^2 w}{\partial r^2} - \frac{\sigma B_0^2}{\rho} w - \frac{\mu}{\rho k_p} w - F_e w^2, \quad (2)$$

$$u \frac{\partial T}{\partial r} + w \frac{\partial T}{\partial z} = \frac{k}{\rho C_p} \left(\frac{\partial^2 T}{\partial r^2} + \frac{1}{r} \frac{\partial T}{\partial r} \right) + \tau \left[D_B \frac{\partial C}{\partial r} \frac{\partial T}{\partial r} + \frac{D_T}{T_\infty} \left(\frac{\partial T}{\partial r} \right)^2 \right] + \frac{\sigma B_0^2}{\rho C_p} w^2 + \frac{1}{\rho C_p} \frac{16\sigma^* T_\infty^3}{3k^*} \frac{\partial^2 T}{\partial r^2}, \quad (3)$$

$$u \frac{\partial C}{\partial r} + w \frac{\partial C}{\partial z} = D_B \left(\frac{\partial^2 C}{\partial r^2} + \frac{1}{r} \frac{\partial C}{\partial r} \right) + \frac{D_T}{T_\infty} \left(\frac{\partial^2 T}{\partial r^2} + \frac{1}{r} \frac{\partial T}{\partial r} \right) - k_r^2 (C - C_\infty) \left(\frac{T}{T_\infty} \right)^{n_1} \exp \left(\frac{-E_a}{kT} \right), \quad (4)$$

with

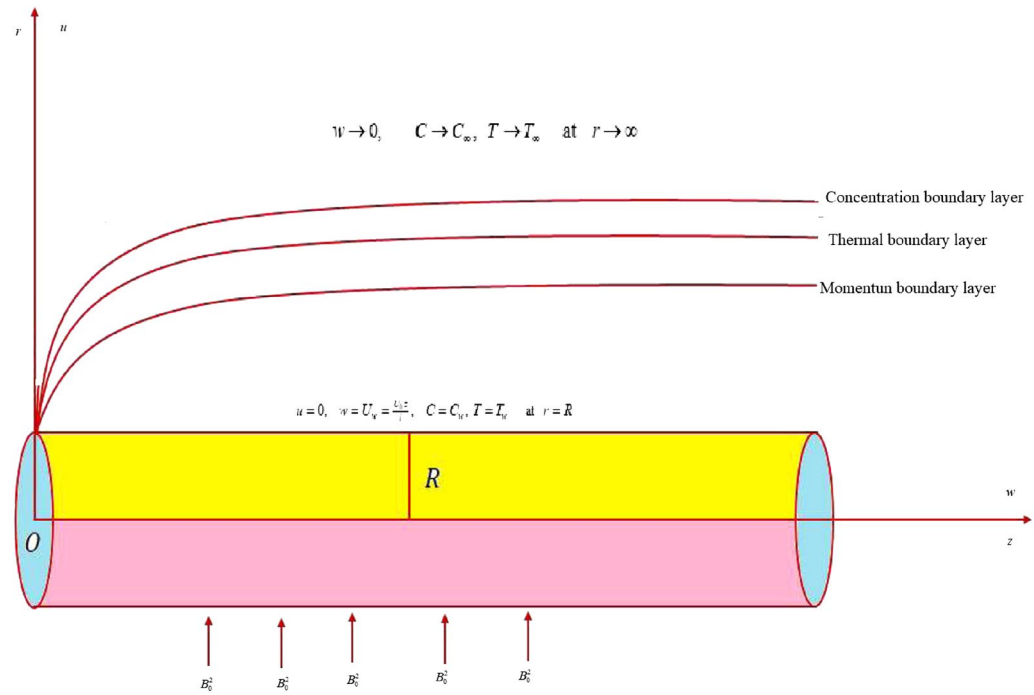


Figure 1. Coordinate system and flow diagram.

$$\left. \begin{aligned} u = 0, w = U_w = \frac{U_0 z}{l}, T = T_w, C = C_w \text{ at } r = R \\ w \rightarrow 0, C \rightarrow C_\infty, T \rightarrow T_\infty \text{ at } r \rightarrow \infty, \end{aligned} \right\} \quad (5)$$

Considering⁵³

$$u = -\sqrt{\frac{\nu U_0}{l}} \frac{R}{r} f(\eta), w = \frac{U_0 z}{l} f'(\eta), \eta = \sqrt{\frac{U_0}{\nu l}} \left(\frac{r^2 - R^2}{2R} \right), \theta(\eta) = \frac{T - T_\infty}{T_w - T_\infty}, \phi(\eta) = \frac{C - C_\infty}{C_w - C_\infty} \quad (6)$$

One has

$$\left. \begin{aligned} (1 + 2\gamma_3 \eta) f'''' + 2\gamma_3 f'' - 2\beta_1 Re \gamma_3 (1 + 2\gamma_3 \eta) f''^2 - 2\beta_1 Re (1 + 2\gamma_3 \eta)^2 f''^2 f'''' \\ - 2\lambda f' - 2M f' - 2Fr f'^2 - 2f'^2 + 2ff'' = 0 \end{aligned} \right\} \quad (7)$$

$$\left. \begin{aligned} (1 + 2\gamma_3 \eta) \theta'' + Pr f \theta' + 2\gamma_3 \theta' + (1 + 2\gamma_3 \eta) Pr Nb \theta' \phi' + (1 + 2\gamma_3 \eta) Pr Nt \theta'^2 \\ + Pr MEc f'^2 + Rd [\gamma_3 \theta' + (1 + 2\gamma_3 \eta) \theta''] = 0 \end{aligned} \right\} \quad (8)$$

$$\left. \begin{aligned} (1 + 2\gamma_3 \eta) \phi'' + \gamma_3 \phi' + \frac{Nt}{Nb} [(1 + 2\gamma_3 \eta) \theta'' + \gamma_3 \theta'] + Sc f \phi' \\ - Sc \gamma \phi (1 + \delta_1 \theta)^{n_1} \exp\left(\frac{-E_1}{1 + \delta_1 \theta}\right) = 0 \end{aligned} \right\} \quad (9)$$

with

$$\left. \begin{aligned} f(0) = 0, \theta(0) = 1, \phi(0) = 1, f'(0) = 1, \\ f'(\infty) = 0, \theta(\infty) = 0, \phi(\infty) = 0. \end{aligned} \right\} \quad (10)$$

Here

$$\left. \begin{aligned} \gamma_3 = \sqrt{\frac{\nu l}{U_0 R^2}}, Re = \frac{U_0 z^2}{\nu l}, M = \sqrt{\frac{\sigma B_0^2 l}{\rho U_0}}, \lambda = \frac{\nu l}{k_p U_0}, \beta_1 = \frac{m B^2 U_0^2}{4 l^2}, Pr = \frac{\mu c_p}{k}, \\ Fr = \frac{C_b}{\sqrt{k_p}}, Rd = \frac{4 \sigma^* T_\infty^3}{k k^*}, Nb = \frac{\tau D_B (C_w - C_\infty)}{\nu}, Nt = \frac{\tau D_T (T_w - T_\infty)}{T_\infty \nu}, \\ \delta_1 = \frac{T_w - T_\infty}{T_\infty}, Ec = \frac{U_w^2}{C_p (T_w - T_\infty)}, E_1 = \frac{E_a}{k T_\infty}, \gamma = \frac{k^2 l}{U_0}, Sc = \frac{\nu}{D_B} \end{aligned} \right\} \quad (11)$$

Physical quantities

Physical quantities are as follows;

$$Cf_z = \frac{-(\tau_w)_{r=R}}{\rho u_w^2}, Nu_z = \frac{zq_w}{k(T_w - T_\infty)}, Sh_z = \frac{zq_m}{D_B(C_w - C_\infty)} \cdot \} \tag{12}$$

where

$$q_w = -k \left(\frac{\partial T}{\partial y} + \frac{16\sigma^* T_\infty^3}{kk^*} \right) \left(\frac{\partial T}{\partial r} \right)_{r=R}, q_m = -D_B \left(\frac{\partial C}{\partial r} \right)_{r=R} \cdot \} \tag{13}$$

Final forms are

$$Cf_z(Re_z)^{\frac{1}{2}} = -f''(0) - \frac{\beta_1}{4} f''(0) [4f'(0) + 4\gamma_3^2 f(0)]^2 - 4f(0)f'(0) + \lambda [f''(0)]^2 \} \tag{14}$$

$$Nu_z(Re_z)^{-\frac{1}{2}} = -[1 + Rd]\theta'(0), Sh_z(Re_z)^{-\frac{1}{2}} = -\phi'(0),$$

where $Re_z \left(= \frac{zU_w}{\nu} \right)$ is local Reynolds number.

Entropy modeling

It is defined as^{52,53};

$$E_G = \frac{k}{T_\infty^2} (1 + Rd) \left(\frac{\partial T}{\partial r} \right)^2 + \frac{\mu}{T_\infty k_p} w^2 + \frac{RD}{T_\infty} \left(\frac{\partial T}{\partial r} \right) \left(\frac{\partial C}{\partial r} \right) + \frac{\sigma B_0^2}{T_\infty} w^2 + \frac{RD}{C_\infty} \left(\frac{\partial C}{\partial r} \right)^2, \tag{15}$$

non-dimensional form of entropy generation rate is

$$S_G = \frac{E_G}{E_{G0}} = (1 + Rd)[1 + 2\gamma_3\eta]\delta_1\theta'^2 + MB_r f'^2 + (1 + 2\gamma_3\eta)L\theta'\phi' \} \tag{16}$$

$$+ (1 + 2\gamma_3\eta)L\frac{\alpha_2}{\delta_1}\phi'^2 + B_r\lambda f'^2,$$

Bejan number is

$$Be = \frac{(1 + Rd)[1 + 2\gamma_3\eta]\delta_1\theta'^2 + (1 + 2\gamma_3\eta)L\theta'\phi'}{(1 + Rd)[1 + 2\gamma_3\eta]\delta_1\theta'^2 + MB_r f'^2 + (1 + 2\gamma_3\eta)L\theta'\phi' \} \tag{17}$$

$$+ (1 + 2\gamma_3\eta)L\frac{\alpha_2}{\delta_1}\phi'^2 + B_r\lambda f'^2,$$

here $S_G \left(= \frac{E_G T_\infty \nu l}{U_0 k (T_w - T_\infty)} \right)$ denotes the entropy rate, $E_{G0} \left(= \frac{k(T_w - T_\infty)}{T_\infty} \left(\frac{U_0}{\nu l} \right) \right)$ the characteristic entropy rate, $B_r \left(= \frac{\mu U_0^2 z^2}{l^2 k (T_w - T_\infty)} \right)$ Brinkman number, $L \left(= \frac{RD(C_w - C_\infty)}{k} \right)$ diffusion variable and $\alpha_2 \left(= \frac{C_w - C_\infty}{C_\infty} \right)$ concentration difference ratio variable.

Numerical solution and discussion

Here NDSolve code in Mathematica is executed to solve the dimensionless system of equations. Impact of sundry variables on Sutterby nanofluid velocity ($f'(\eta)$), thermal field ($\theta(\eta)$), mass concentration ($\phi(\eta)$) EG rate (S_G) and Bejan number (Be) are scrutinized by plotting. Engineering quantities are evaluated numerically. Table 1 is labeled to ensure the correctness of present numerical approach. This table demonstrated the comparison of gradients of temperature ($\theta''(0)$) versus different Pr values while influence of remaining variables is neglected. Clearly the results are in good agreement.

Velocity

Figure 2 delineates Sutterby fluid parameter (β_1) impact on $f'(\eta)$. For raising values of β_1 velocity decreases. Physically for raising β_1 relaxation time increases as a result viscous effects dominants therefore additional resistance is offered to fluid particles thus $f'(\eta)$ decreases. Figure 3 discovers influence of Forchheimer variable

Pr	Present results	Wang ⁵⁴	Gorla and Sidawi ⁵⁵
0.07	0.0645	0.0656	0.06562
0.20	0.1689	0.1691	0.1691
0.70	0.4538	0.4539	0.53488
2.00	0.9113	0.9114	0.91142
7.00	1.8953	1.8954	1.89046
20.00	3.3539	3.3539	3.35391

Table 1. Comparison of results for gradient of temperature.

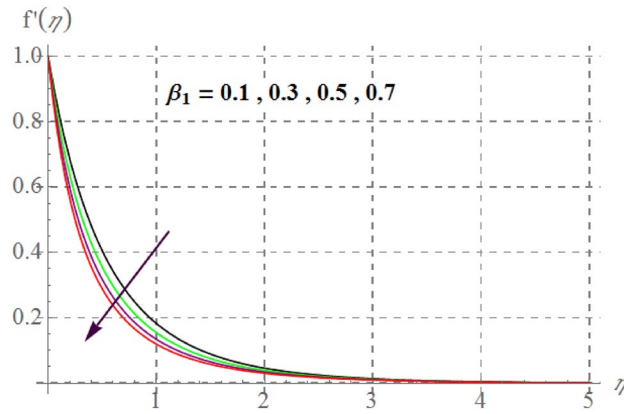


Figure 2. $f'(\eta)$ curves versus β_1 .

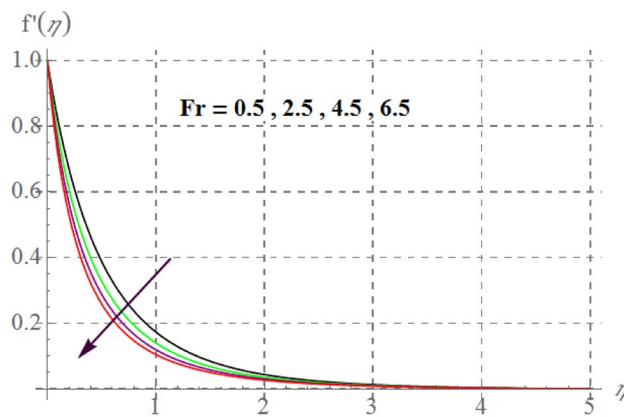


Figure 3. $f'(\eta)$ curves via Fr .

(Fr) on fluid velocity. Physically, for hiking Fr estimations, $f'(\eta)$ decreases. For larger values of Fr drag surface force increases, thus $f'(\eta)$ decreases. Figure 4 shows influence of γ_3 on $f'(\eta)$. here, material velocity upsurges via rising γ_3 . For higher γ_3 cylinder radius decreases as a result fluid contact area between fluid particles and surface of cylinder decreases due to which less resistive force of surface is offered to fluid particles so velocity upsurges. Figure 5 describes influence of surface porosity on $f'(\eta)$. Velocity decreases for improvement in λ . For increasing values of λ kinematic viscosity of porous medium upsurges, therefore $f'(\eta)$ curves decays. Behavior of $f'(\eta)$ versus magnetic variable is captured in Fig. 6. Velocity diminishes versus higher M . Since through higher M Lorentz force enhances which acts in the opposite direction of flow and thus velocity decays. From Fig. 7

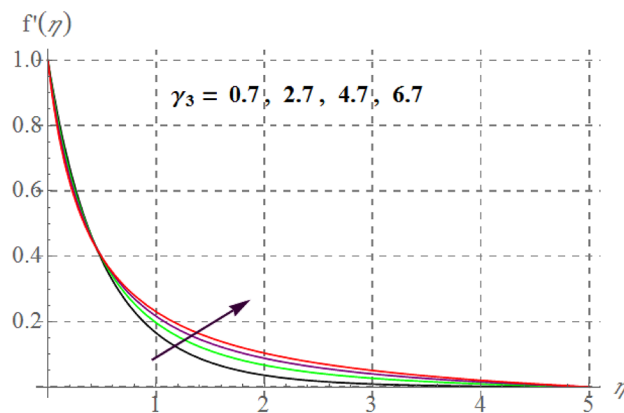


Figure 4. $f'(\eta)$ curves through γ_3 .

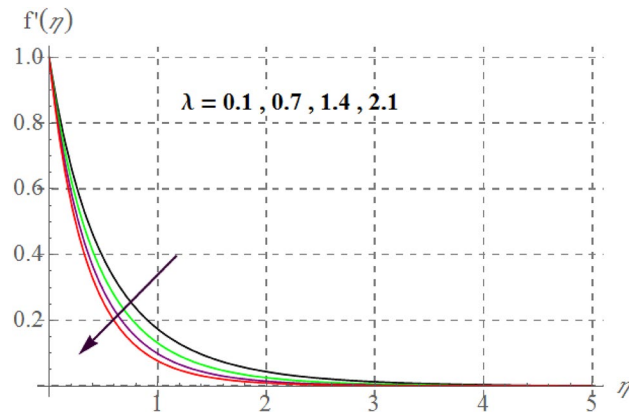


Figure 5. $f'(\eta)$ curves against λ .

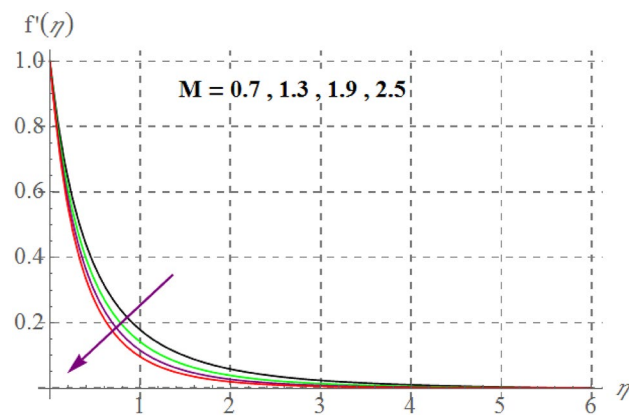


Figure 6. $f'(\eta)$ curves versus M .

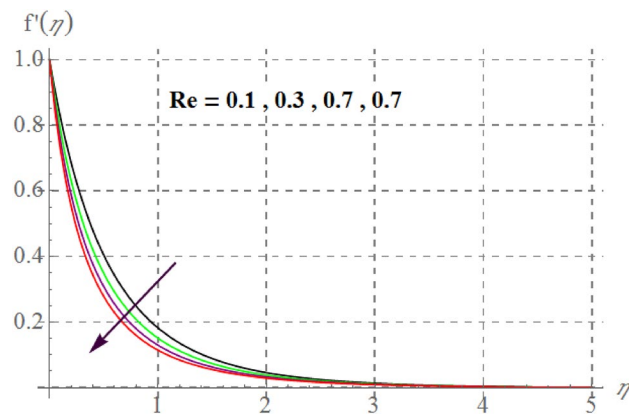


Figure 7. $f'(\eta)$ curves via Re .

it is noticed that Re and $f'(\eta)$ have an inverse relation. In fact Re has direct and inverse relations with inertial forces and viscous forces, thus for larger Re viscous forces dominant over inertial forces thus velocity decreases.

Temperature

Figure 8 gives inspiration of Ec on $\theta(\eta)$. For enlargement in Ec temperature upturns. Since for higher Ec , internal energy of fluid boosts, consequently kinetic energy of system increases as a result inside friction of tiny solid particles enhances and extra heat supplied to the system, resultantly $\theta(\eta)$ increases. Variation in thermal fluid versus γ_3 is captured in Fig. 9. Clearly $\theta(\eta)$ increases for raising values of γ_3 . Figure 10 shows the variation in

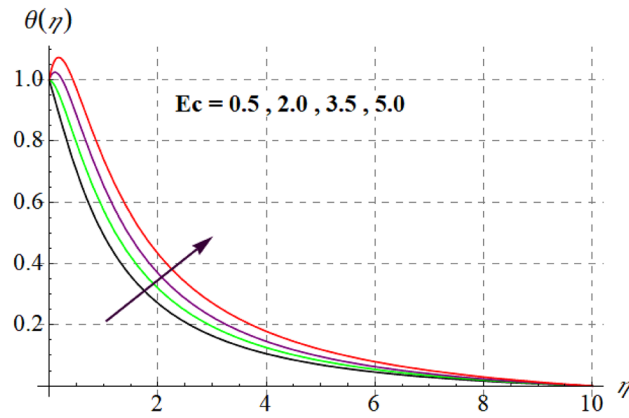


Figure 8. $\theta(\eta)$ curves against Ec .

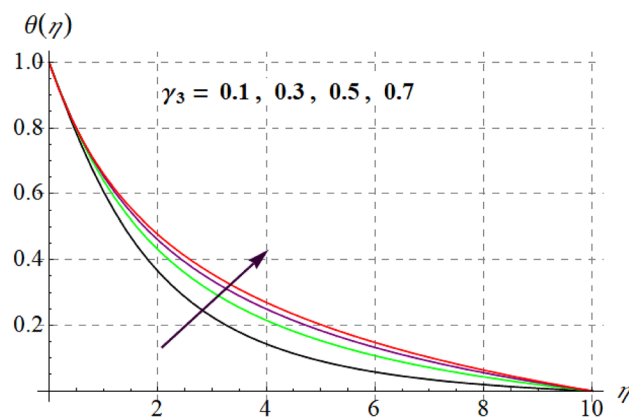


Figure 9. $\theta(\eta)$ curves versus γ_3 .

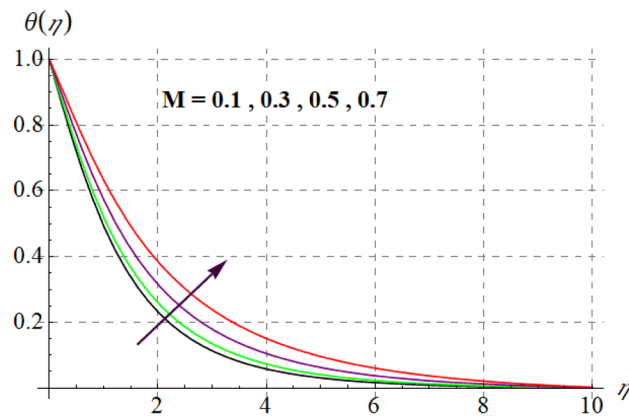


Figure 10. $\theta(\eta)$ curves via M .

$\theta(\eta)$ against M . For greater estimations of M temperature rises. In fact more heat is added in the system when magnetic variable amplifies due to resistive force and so $\theta(\eta)$ increases. Influence of Nb on $\theta(\eta)$ is checked in Fig. 11. Temperature improves through higher Nb . Random movement of tiny particles increases with in fluid against higher Nb , consequently inter collision of nanoparticles increases and thus extra heat generates, therefore $\theta(\eta)$ improves. Figure 12 is designed to check the outcome of Nt on $\theta(\eta)$. For raising Nt thermal field boosts. Physically, when thermophoresis force increases rate of shifting of solid tiny particles from hot to cold region improves, so $\theta(\eta)$ escalates. Figure 13 articulates the influence of Pr on thermal field. It is perceived here that via higher Pr thermal field declines. Physically through rising Pr fluid thermal diffusivity diminished and thus $\theta(\eta)$

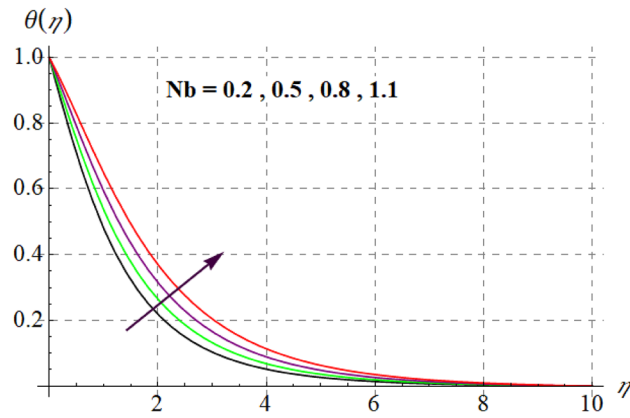


Figure 11. $\theta(\eta)$ curves versus Nb .

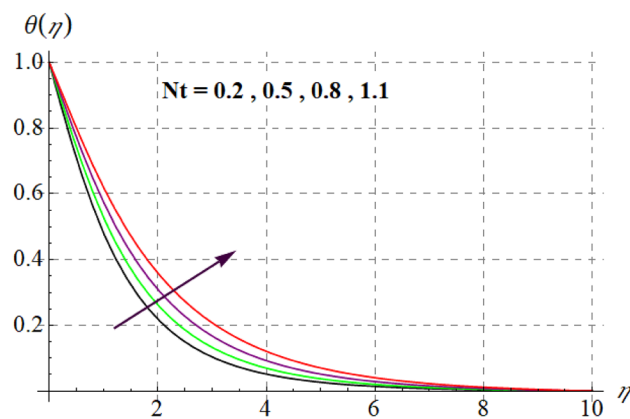


Figure 12. $\theta(\eta)$ curves against Nt .

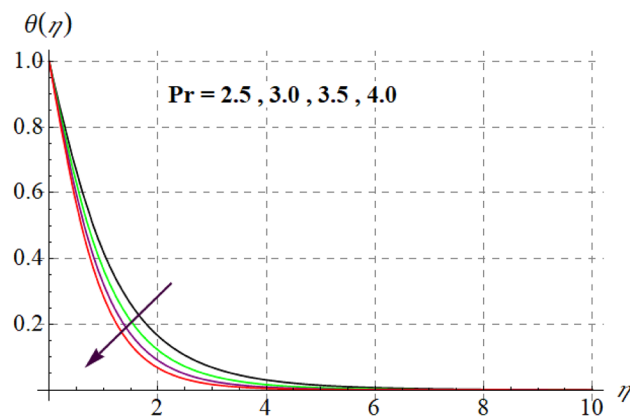


Figure 13. $\theta(\eta)$ curves versus Pr .

retards. Influence of radiation variable on $\theta(\eta)$ is given in Fig. 14. Here $\theta(\eta)$ boosts via larger Rd . since surface heat flux boosts for higher values of Rd and thus $\theta(\eta)$ improves.

Concentration

Figure 15 is drafted to show influence of δ_1 on $\phi(\eta)$. It is observed that for an escalation in δ_1 values $\phi(\eta)$ upsurges. Figure 16 depicts E_1 effect on $\phi(\eta)$ Concentration upsurges for raising values of E_1 . For higher E_1 Arrhenius function decreases thus concentration increases. Figure 17 portrays effect of γ on $\phi(\eta)$. Concentration decreases for raising γ . For higher γ destructive rate of reaction increases and thus liquid species liquefy more successfully, so

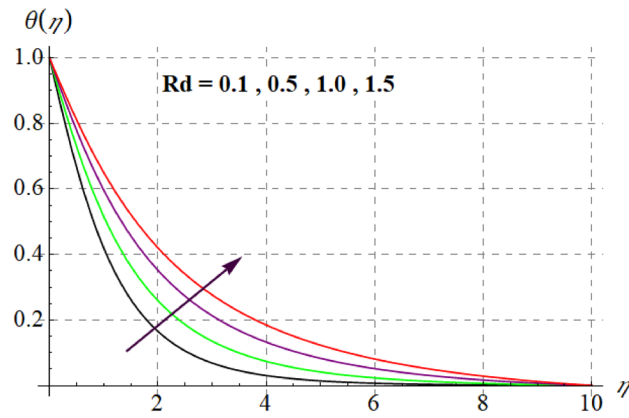


Figure 14. $\theta(\eta)$ curves versus Rd .

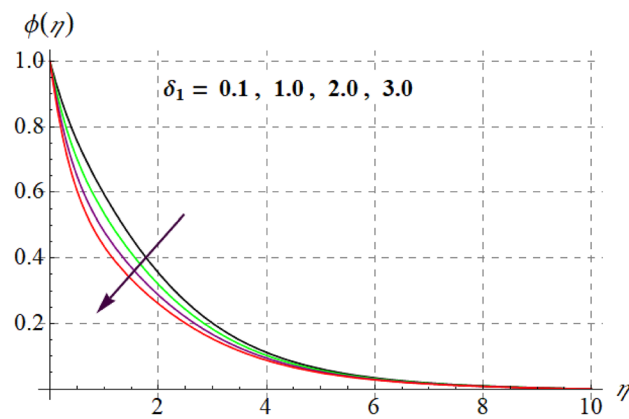


Figure 15. $\phi(\eta)$ curves versus δ_1 .

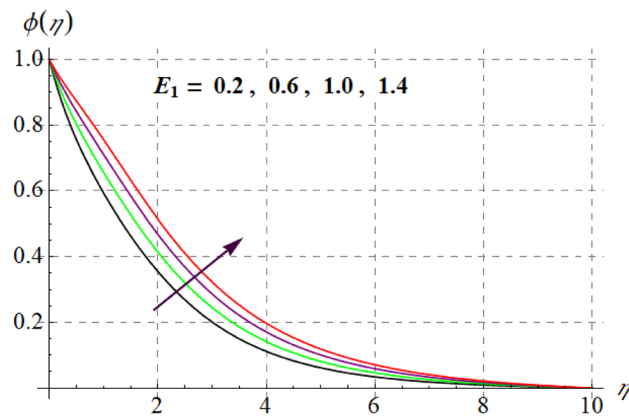


Figure 16. $\phi(\eta)$ curves versus E_1 .

$\phi(\eta)$ decreases. Figure 18 gives impact of γ_3 on $\phi(\eta)$. For enlargement in γ_3 concentration increases. Figure 19 expresses the Nb influence on $\phi(\eta)$. Nanofluid mass concentration declines through rising Nb . Physically, intermolecular collision boosts against higher Nb due to arbitrary movement. Resultantly more heat generates thus temperature increases and $\phi(\eta)$ decreases. Figure 20 explores the behavior of $\phi(\eta)$ versus Nt . Fluid concentration increases for higher values of Nt . Physically, thermophoretic force which shifts fluid particles from hot to cold region increases for enlargement in Nt thus $\phi(\eta)$ increases. Figure 21 is plotted to study influence of Sc on $\phi(\eta)$. Here, $\phi(\eta)$ decreases via increasing values of Sc . Since mass diffusivity reduces for larger Schmidt number and thus $\phi(\eta)$ is diminished.

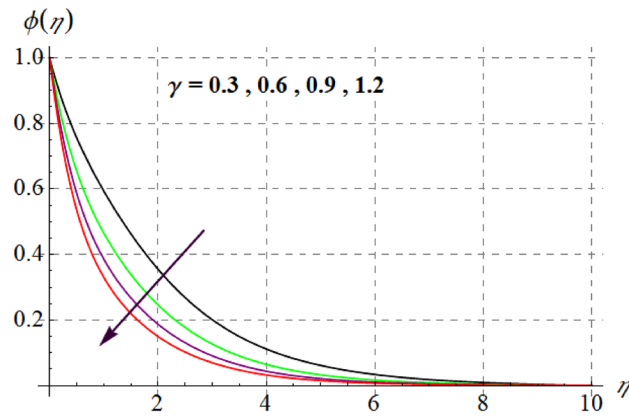


Figure 17. $\phi(\eta)$ curves versus γ .

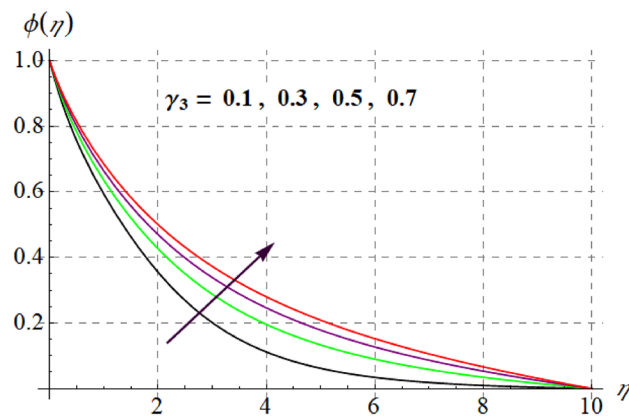


Figure 18. $\phi(\eta)$ curves versus γ_3 .

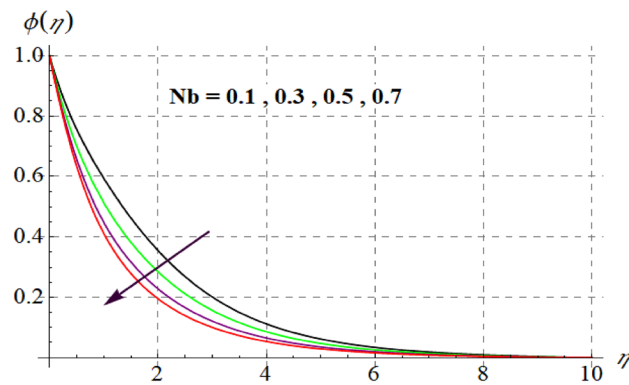


Figure 19. $\phi(\eta)$ curves via Nb .

Entropy generation and Bejan number

This section is devoted to check the influences of Br , δ_1 and M on S_G and Be . Figures 22 and 23 portrays Br influence on S_G and Be . For higher Br values S_G increases while Be decays. Physically, Br acts as heat source within the fluid. Therefore higher Br produces more heat and thus S_G enhances whereas Be decays. Figures 24 and 25 shows influence of δ_1 on S_G and Be . For higher δ_1 values irreversibility enhances thus both S_G and Be increased. Since δ_1 is in direct relation with $T_w - T_\infty$ and we know that $T_w > T_\infty$, so higher δ_1 produces more heat to the fluid and thus both S_G and Be enhanced. Outcomes of magnetic variable on S_G and Be is expressed in Figs. 26 and 27. It is observed that S_G increases for higher M while opposite behavior holds for Be . It is due to the fact that M is linked with Lorentz force, which is a resistive force and opposes the flow. Consequently irreversibility within in fluid upsurges and Bejan decays.

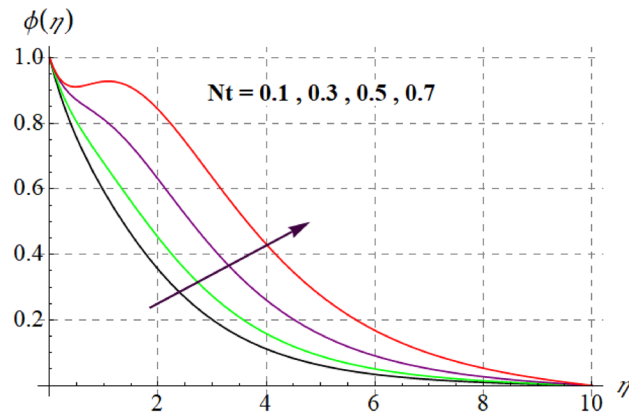


Figure 20. $\phi(\eta)$ curves against Nt .

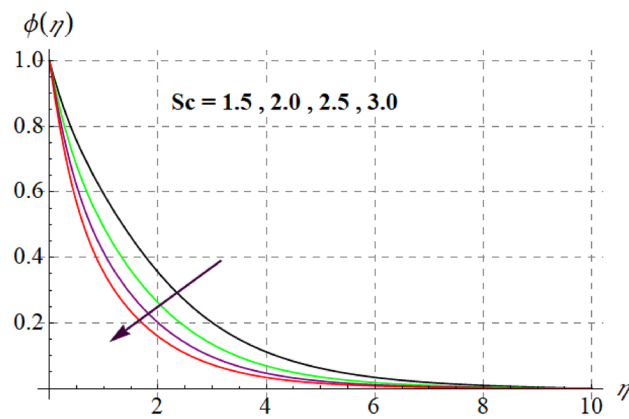


Figure 21. $\phi(\eta)$ curves versus Sc .

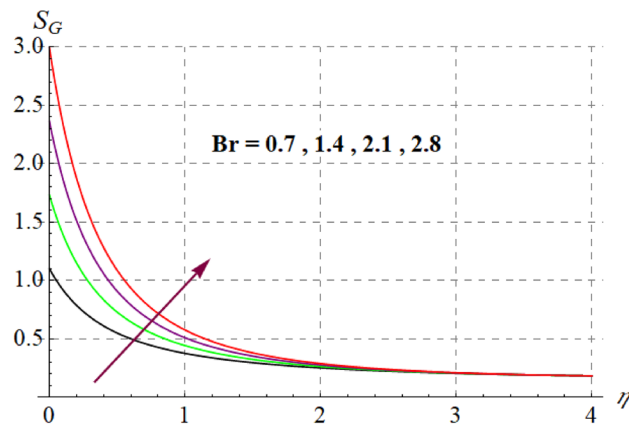


Figure 22. S_G via Br .

Engineering quantities

Here skin friction coefficient $\left(Cf_z(Re_z)^{\frac{1}{2}}\right)$, rate of heat transfer $\left(Nu_z(Re_z)^{-\frac{1}{2}}\right)$ and Sherwood number $\left(Sh_z(Re_z)^{-\frac{1}{2}}\right)$ are discussed numerically. Outcomes of various flow parameters on $Cf_z(Re_z)^{\frac{1}{2}}$ are examined in Table 2. For higher $\beta_1, Fr, \gamma_3, \lambda, M$, and Re velocity gradient improves. Computational results of Nusselt number for different flow variables are given in Table 3. Clearly noted that for higher Pr, M, Nt, Nb and Ec temperature gradient decreases. An augmentation in Nu_z is seen for Rd and γ_3 . Variation of various sundry variables on mass

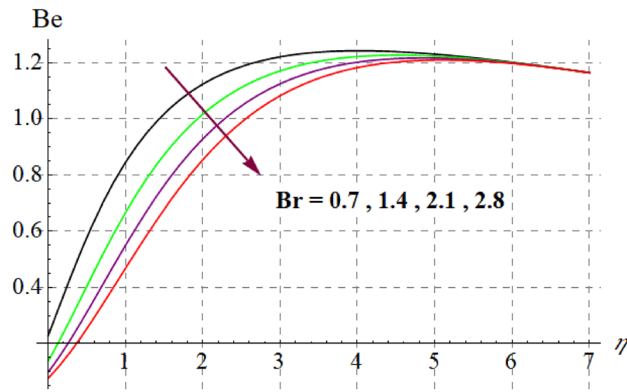


Figure 23. *Be* against *Br*.

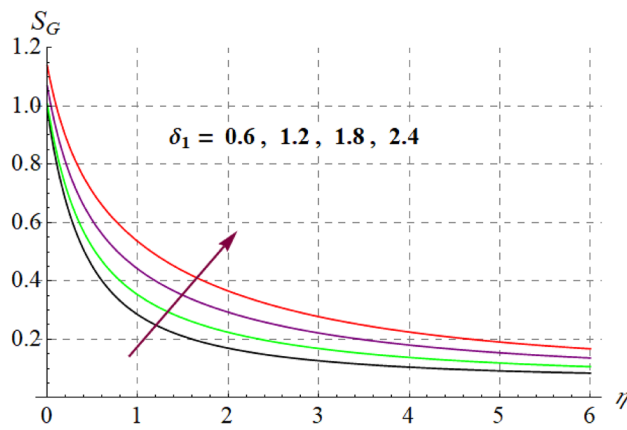


Figure 24. *S_G* via δ_1 .

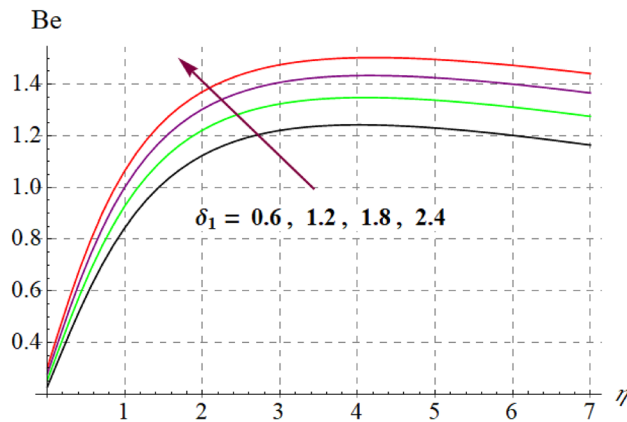


Figure 25. *Be* versus δ_1 .

transfer rate is examined in Table 4. From this table it is observed that Sherwood number improves for higher $\delta_1, \gamma, n, Nb, Nt$ and Sc . Opposite effect is seen for E_1 and γ_3 .

Conclusions

The prime objective of this article is to examine the irreversibility in steady magnetized flow of Sutterby nanofluid caused by stretched cylinder. The features of Arrhenius kinetics, Joule heating, chemical reaction, Darcy Forchheimer, surface permeability and thermal radiation are accounted in development of mathematical governing

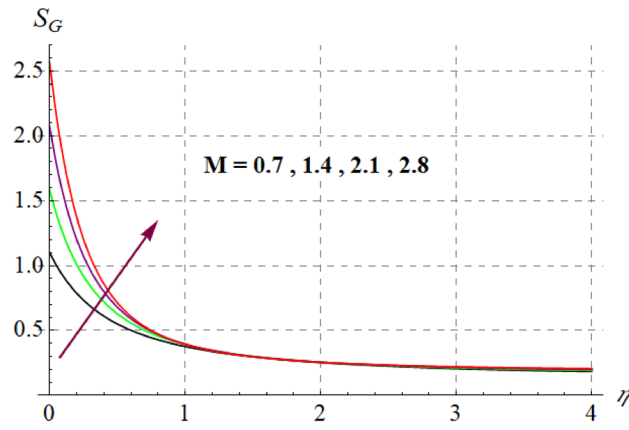


Figure 26. S_G via M .

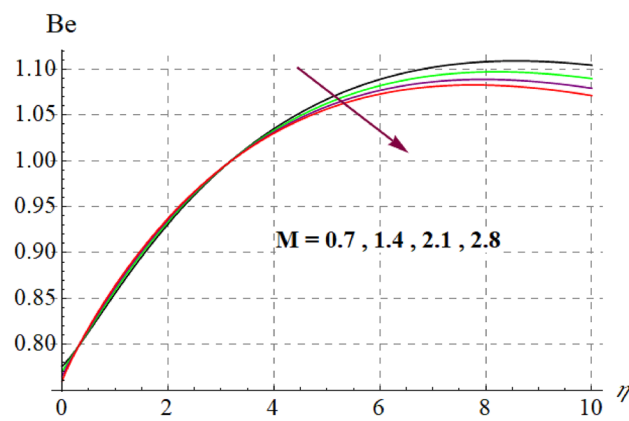


Figure 27. Be against M .

β_1	Fr	γ_3	λ	M	Re	$Cf_z (Re_z)^{\frac{1}{2}}$
0.6	0.5	0.7	0.2	0.7	0.01	0.232204
0.7						0.487635
0.8						0.745848
	0.5					0.232204
	0.7					0.271123
		0.7				0.232204
		0.9				0.288469
			0.2			0.232204
			0.4			1.62164
				0.7		0.232204
				0.9		0.295894
					0.01	0.232204
					0.02	0.279904

Table 2. Numerical simulations for $Cf_z (Re_z)^{\frac{1}{2}}$.

equations. Through thermodynamics 2nd law total irreversibility is modeled. Numerical and graphical solutions are constructed through RKF-45 in Mathematica package. Main findings are itemized as:

- Velocity decreases for higher porosity parameter and magnetic variable.
- Temperature have opposite behavior for magnetic variable and Prandtl number.
- For higher thermophoresis and Brownian movement variable temperature enhances.

Ec	γ_3	M	Nb	Nt	Pr	Rd	$Nu_z(Re_z)^{-\frac{1}{2}}$
0.5	0.7	0.7	0.5	0.5	1.5	1.0	0.692796
0.6							0.671870
0.7							0.650944
	0.7						0.692796
	0.9						0.773657
		0.7					0.692796
		0.8					0.677195
			0.5				0.692796
			0.6				0.65948
				0.5			0.692796
				0.6			0.665348
					1.5		0.692796
					1.6		0.677874
						1.0	0.692796
						1.1	0.72645

Table 3. Numerical simulations for $Nu_z(Re_z)^{-\frac{1}{2}}$.

δ_1	E_1	γ_3	γ	n	Nb	Nt	Sc	$Sh_z(Re_z)^{-\frac{1}{2}}$
0.6	0.5	0.7	0.5					0.665558
0.7								0.682322
0.8								0.698943
	0.5							0.665558
	0.8							0.619483
		0.7						0.665558
		0.9						0.66453
			0.5					0.665558
			0.7					0.758014
				1.0				0.665558
				2.0				0.773672
					0.5			0.665558
					0.6			0.678996
						0.5		0.665558
						0.6		0.680346
							0.6	0.665558
							0.8	0.766182

Table 4. Numerical simulations for $Sh_z(Re_z)^{-\frac{1}{2}}$.

- Concentration decreases for Brownian movement variable while it increases for thermophoresis variable.
- For higher Schmidt number concentration decreases.
- EG increases for higher Brinkman number, temperature difference ratio variable and magnetic variable.
- Bejan number decays versus higher Brinkman number and magnetic variable while it enhances for temperature difference ratio variable.

Data availability

All data generated or analyzed during this study are included in this published article.

Received: 2 June 2023; Accepted: 1 November 2023

Published online: 03 November 2023

References

1. John Sutterby, L. Laminar converging flow of dilute polymer solutions in conical section. II. *Trans. Soc. Rheol.* **9**, 227–241. <https://doi.org/10.1122/1.549024> (1965).

2. Naveed, I., Maryyam, J., Muhammad, S., Phatiphat, T. & Zahra, A. Theoretical exploration of thermal transportation with chemical reactions for Sutterby fluid model obeying peristaltic mechanism. *J. Mater. Res. Technol.* **9**, 7449–7459. <https://doi.org/10.1016/j.jmrt.2020.04.071> (2020).
3. Hayat, T., Hinar, Z., Mustafa, M. & Alsaedi, A. Peristaltic flow of Sutterby fluid in a vertical channel with radiative heat transfer and compliant walls: A numerical study. *Results Phys.* **6**, 805–810. <https://doi.org/10.1016/j.rinp.2016.10.0155> (2016).
4. Akbar, N. S. & Nadeem, S. Nano Sutterby fluid model for the peristaltic flow in small intestines. *J. Comput. Theor. Nanosci.* **10**, 2491–2499. <https://doi.org/10.1166/jctn.2013.3238> (2013).
5. Batra, R. L. & Eissa, M. Helical flow of a Sutterby model fluid. *Polym.-Plast. Technol. Eng.* **33**(4), 489–501. <https://doi.org/10.1080/03602559408010743> (1994).
6. Ishtiaq, B., Nadeem, S. & Alzabut, J. Effects of variable magnetic field and partial slips on the dynamics of Sutterby nanofluid due to biaxially exponential and nonlinear stretchable sheets. *Heliyon* **9**(7), e17921. <https://doi.org/10.1016/j.heliyon.2023.e17921> (2023).
7. Azam, M., Khan, W. A., Nayak, M. K. & Majeed, A. Three dimensional convective flow of Sutterby nanofluid with activation energy. *Case Stud. Therm. Eng.* **50**, 103446. <https://doi.org/10.1016/j.csite.2023.103446> (2023).
8. Khan, W. A. *et al.* Impact of stratification phenomena on a nonlinear radiative flow of sutterby nanofluid. *J. Market. Res.* **15**, 306–314. <https://doi.org/10.1016/j.jmrt.2021.08.011> (2021).
9. Choi, S. U. S. & Eastman, J. A. Enhancing thermal conductivity of fluids with nanoparticles. *ASME Publ.-Fed.* **231**, 99–106 (1995).
10. Buongiorno, J. Convective transport in nanofluids. *J. Heat Transf.* **128**, 240–250 (2006).
11. Prasad, P. D., Kumar, R. V. M. S. S. K. & Varma, S. V. K. Heat and mass transfer analysis for the MHD flow of nanofluid with radiation absorption. *Ain. Sham. Eng. J.* **9**, 801–813. <https://doi.org/10.1115/1.2150834> (2018).
12. Turkyilmazoglu, M. On the transparent effects of Buongiorno nanofluid model on heat and mass transfer. *Eur. Phys. J. Plus* **136**, 376. <https://doi.org/10.1140/epjp/s13360-021-01359-2> (2021).
13. Tian, X. Y., Li, B. W. & Hu, Z. M. Convective stagnation point flow of a MHD non-Newtonian nanofluid towards a stretching plate. *Int. J. Heat Mass Transf.* **127**, 768–780. <https://doi.org/10.1016/j.ijheatmasstransfer.2018.07.033> (2018).
14. Turkyilmazoglu, M. Exact solutions concerning momentum and thermal fields induced by a long circular cylinder. *Eur. Phys. J. Plus* **136**, 483. <https://doi.org/10.1140/epjp/s13360-021-01500-1> (2021).
15. Hayat, T., Qayyum, S., Imtiaz, M. & Alsaedi, A. Comparative study of silver and copper water nanofluids with mixed convection and nonlinear thermal radiation. *Int. J. Heat Mass Transf.* **102**, 723–732. <https://doi.org/10.1016/j.ijheatmasstransfer.2016.06.059> (2016).
16. Awan, S. E. *et al.* Numerical computing paradigm for investigation of micropolar nanofluid flow between parallel plates system with impact of electrical MHD and Hall current. *Arab. J. Sci. Eng.* **46**(1), 645–662. <https://doi.org/10.1007/s13369-020-04736-8> (2020).
17. Hussain, A. *et al.* Heat transmission of engine-oil-based rotating nanofluids flow with influence of partial slip condition: A computational model. *Energies* **14**(13), 3859. <https://doi.org/10.1016/j.csite.2021.101500> (2021).
18. Qureshi, I. H. *et al.* Influence of radially magnetic field properties in a peristaltic flow with internal heat generation: Numerical treatment. *Case Stud. Therm. Eng.* **26**, 101019. <https://doi.org/10.1016/j.csite.2021.101019> (2021).
19. Parveen, N. *et al.* Influence of radially magnetic field properties in a peristaltic flow with internal heat generation: Numerical treatment. *Case Stud. Therm. Eng.* **26**, 101019. <https://doi.org/10.1016/j.csite.2021.101285> (2021).
20. Khan, W. U. *et al.* Novel mathematical modeling with solution for movement of fluid through ciliary caused metachronal waves in a channel. *Sci. Rep.* <https://doi.org/10.1038/s41598-021-00039-6> (2021).
21. Awan, S. E. *et al.* Convective flow dynamics with suspended carbon nanotubes in the presence of magnetic dipole: Intelligent solution predicted Bayesian regularization networks. *Tribol. Int.* **187**, 108685. <https://doi.org/10.1016/j.triboint.2023.108685> (2023).
22. Awan, S. E., Raja, M. A. Z., Awais, M. & Shu, C.-M. Intelligent Bayesian regularization networks for bio-convective nanofluid flow model involving gyro-tactic organisms with viscous dissipation, stratification and heat immersion. *Eng. Appl. Comput. Fluid Mech.* **15**(1), 1508–1530. <https://doi.org/10.1080/19942060.2021.1974946> (2021).
23. Awan, S. E., Ali, F., Awais, M., Shoaib, M. & Raja, M. A. Z. Intelligent Bayesian regularization-based solution predictive procedure for hybrid nanoparticles of AA7072-AA7075 oxide movement across a porous medium. *Z. Angew. Math. Mech.* <https://doi.org/10.1002/zamm.202300043> (2023).
24. Ahmed, J., Khan, M. & Ahmad, L. Stagnation point flow of Maxwell nanofluid over a permeable rotating disk with heat source/sink. *J. Mol. Liq.* **287**, 110853. <https://doi.org/10.1016/j.molliq.2019.04.130> (2019).
25. Hsiao, K.-L. Combined electrical MHD heat transfer thermal extrusion system using Maxwell fluid with radiative and viscous dissipation effects. *Appl. Therm. Eng.* **112**, 1281–1288. <https://doi.org/10.1016/j.applthermaleng.2016.08.208> (2017).
26. Hassan, A., Hussain, A., Arshad, M., Alanazi, M. M. & Zahran, H. Y. Numerical and thermal investigation of magneto-hydrodynamic hybrid nanoparticles (SWCNT-Ag) under Rosseland radiation: A prescribed wall temperature case. *Nanomaterials* **12**(6), 891. <https://doi.org/10.3390/nano1206089> (2022).
27. Hassan, A. *et al.* Heat transport investigation of hybrid nanofluid (Ag-CuO) porous medium flow: Under magnetic field and Rosseland radiation. *Ain Shams Eng. J.* **13**(5), 101667. <https://doi.org/10.1016/j.asej.2021.101667> (2022).
28. Harish, R. & Sivakumar, R. Effects of nanoparticle dispersion on turbulent mixed convection flows in cubical enclosure considering Brownian motion and thermophoresis. *Powder. Technol.* **378**, 303–316. <https://doi.org/10.1016/j.powtec.2020.09.054> (2021).
29. Pakravan, H. A. & Yaghoubi, M. Combined thermophoresis, Brownian motion and Dufour effects on natural convection of nanofluids. *Int. J. Ther. Sci.* **50**, 394–402. <https://doi.org/10.1016/j.ijthermalsci.2010.03.007> (2011).
30. Hussain, A., Rehman, A., Nadeem, S., Khan, M. R. & Issakhov, A. A computational model for the radiated kinetic molecular postulate of fluid-originated nanomaterial liquid flow in the induced magnetic flux regime. *Math. Probl. Eng.* <https://doi.org/10.1155/2021/6690366> (2021).
31. Seddeek, M. A. Influence of viscous dissipation and thermophoresis on Darcy-Forchheimer mixed convection in a fluid saturated porous media. *J. Colloid Interface Sci.* **293**, 137–142. <https://doi.org/10.1016/j.jcis.2005.06.039> (2006).
32. Umavathi, J. C., Ojjela, O. & Vajravelu, K. Numerical analysis of natural convective flow and heat transfer of nanofluids in a vertical rectangular duct using Darcy–Forchheimer–Brinkman model. *Int. J. Therm. Sci.* **111**, 511–524. <https://doi.org/10.1016/j.ijthermalsci.2016.10.002> (2017).
33. Muhammad, T., Alsaedi, A., Shehzad, S. A. & Hayat, T. A revised model for Darcy Forchheimer flow of Maxwell nanofluid subject to convective boundary condition. *Chin. J. Phys.* **55**, 963–976. <https://doi.org/10.1016/j.cjph.2017.03.006> (2017).
34. Hayat, T., Rafique, K., Muhammad, T., Alsaedi, A. & Ayub, M. Carbon nanotubes significance in Darcy-Forchheimer flow. *Results Phys.* **8**, 26–33. <https://doi.org/10.1016/j.rinp.2017.11.022> (2018).
35. Alzahrani, A. K. Importance of Darcy-Forchheimer porous medium in 3D convective flow of carbon nanotubes. *Phys. Lett. A.* **382**, 2938–2943. <https://doi.org/10.1016/j.physleta.2018.06.030> (2018).
36. Turkyilmazoglu, M. Flow and heat over a rotating disk subject to a uniform horizontal magnetic field. *Zeitschrift für Naturforschung A* **77**(4), 329–337. <https://doi.org/10.1515/zna-2021-0350> (2022).
37. Hayat, T., Aziz, A., Muhammad, T. & Alsaedi, A. An optimal analysis for Darcy Forchheimer 3D flow of Carreau nanofluid with convectively heated surface. *Results Phys.* **9**, 598–608. <https://doi.org/10.1016/j.rinp.2018.03.009> (2018).
38. Bestman, A. R. Natural convection boundary layer with suction and mass transfer in a porous medium. *Int. J. Energy Res.* **14**, 389–396. <https://doi.org/10.1002/er.4440140403> (1990).

39. Makinde, O. D., Olanrewaju, P. O. & Charles, W. M. Unsteady convection with chemical reaction and radiative heat transfer past a flat porous plate moving through a binary mixture. *J. Afrika Matematika*. **22**, 65–78. <https://doi.org/10.1007/s13370-011-0008-z> (2011).
40. Maleque, K. A. Effects of binary chemical reaction and activation energy on MHD boundary layer heat and mass transfer flow with viscous dissipation and heat generation/absorption. *J. Hindawi Publ. Corp ISRN Thermodyn*. **2013**, 284637. <https://doi.org/10.1155/2013/284637> (2013).
41. Awad, F. G., Motsa, S. & Khumalo, M. Heat and mass transfer in unsteady rotating fluid flow with binary chemical reaction and activation energy. *PLoS ONE*. **9**, 0107622. <https://doi.org/10.1371/journal.pone.0107622> (2014).
42. Hsiao, K.-L. To promote radiation electrical MHD activation energy thermal extrusion manufacturing system efficiency by using Carreau-Nanofluid with parameters control method. *Energy* **130**, 486–499. <https://doi.org/10.1016/j.energy.2017.05.004> (2017).
43. Bejan, A. Entropy generation minimization: The new thermodynamics of finite-size devices and finite-time processes. *J. Appl. Phys.* **79**, 1191–1218. <https://doi.org/10.1063/1.362674> (1996).
44. Turkyilmazoglu, M. Velocity slip and entropy generation phenomena in thermal transport through metallic porous channel. *J. Non-Equilib. Thermodyn.* **45**, 247–256. <https://doi.org/10.1515/jnet-2019-0097> (2020).
45. Khan, M. I., Qayyum, S., Hayat, T., Alsaedi, A. & Khan, M. I. Investigation of Sisko fluid through entropy generation. *J. Mol. Liq.* **257**, 155–163. <https://doi.org/10.1016/j.molliq.2018.02.087> (2018).
46. Vatanmakan, M., Lakzian, E. & Mahpeykar, M. R. Investigating the entropy generation in condensing steam flow in turbine blades with volumetric heating. *Energy* **147**, 701–714. <https://doi.org/10.1016/j.energy.2018.01.097> (2018).
47. Khan, M. I. *et al.* Entropy generation minimization and binary chemical reaction with Arrhenius activation energy in MHD radiative flow of nanomaterial. *J. Mol. Liq.* **259**, 274–283. <https://doi.org/10.1016/j.molliq.2018.03.049> (2018).
48. Gul, A., Khan, I. & Makhanov, S. S. Entropy generation in a mixed convection Poiseuille flow of molybdenum disulphide Jeffrey nanofluid. *Results Phys.* **9**, 947–954. <https://doi.org/10.1016/j.rinp.2018.03.012> (2018).
49. Xie, Z. Y. & Jian, Y. J. Entropy generation of two-layer magnetohydrodynamic electroosmotic flow through microparallel channels. *Energy* **139**, 1080–1093 (2017).
50. Khan, M. I., Ullah, S., Hayat, T., Khan, M. I. & Alsaedi, A. Entropy generation minimization (EGM) for convection nanomaterial flow with nonlinear radiative heat flux. *J. Mol. Liq.* **260**, 279–291. <https://doi.org/10.1016/j.energy.2017.08.038> (2018).
51. Humnic, G. & Humnic, A. The heat transfer performances and entropy generation analysis of hybrid nanofluids in a flattened tube. *Int. J. Heat Mass Transf.* **119**, 813–827. <https://doi.org/10.1016/j.ijheatmasstransfer.2017.11.155> (2018).
52. Aldabesh, A., Haredy, A., Al-Khaled, K., Khan, S. U. & Tlili, I. Darcy resistance flow of Sutterby nanofluid with microorganisms with applications of nano-biofuel cells. *Sci. Rep.* **12**, 7514. <https://doi.org/10.1038/s41598-022-11528-7> (2022).
53. Song, Y. Q. *et al.* Bioconvection analysis for Sutterby nanofluid over an axially stretched cylinder with melting heat transfer and variable thermal features: A Marangoni and solutal model. *Alex. Eng. J.* **60**(5), 4663–4675. <https://doi.org/10.1016/j.aej.2021.03.056> (2021).
54. Wang, C. Y. Free convection on a vertical stretching surface. *J. Appl. Math. Mech. (ZAMM)* **69**, 418–420. <https://doi.org/10.1007/BF00853952> (1989).
55. Reddy Gorla, R. S. & Sidawi, I. Free convection on a vertical stretching surface with suction and blowing. *Appl. Sci. Res.* **52**, 247–257. <https://doi.org/10.1007/BF00853952> (1994).

Acknowledgements

Researchers Supporting Project number (RSPD2023R1060), King Saud University, Riyadh, Saudi Arabia.

Author contributions

M.R., F.A.A.: conceived, designed the analysis and wrote the paper text. F.H., E.A.A.I.: contributed the analysis tools. M.I.K.: supervised overall activities.

Competing interests

The authors declare no competing interests.

Additional information

Correspondence and requests for materials should be addressed to F.H.

Reprints and permissions information is available at www.nature.com/reprints.

Publisher's note Springer Nature remains neutral with regard to jurisdictional claims in published maps and institutional affiliations.



Open Access This article is licensed under a Creative Commons Attribution 4.0 International License, which permits use, sharing, adaptation, distribution and reproduction in any medium or format, as long as you give appropriate credit to the original author(s) and the source, provide a link to the Creative Commons licence, and indicate if changes were made. The images or other third party material in this article are included in the article's Creative Commons licence, unless indicated otherwise in a credit line to the material. If material is not included in the article's Creative Commons licence and your intended use is not permitted by statutory regulation or exceeds the permitted use, you will need to obtain permission directly from the copyright holder. To view a copy of this licence, visit <http://creativecommons.org/licenses/by/4.0/>.

© The Author(s) 2023